Surface Inorganic Iodine Speciation in the Indian and Southern Oceans from 12°N to 70°S

Running title: Iodine in the Indian Ocean

Rosie J. Chance[1*+], Liselotte Tinel[1+], Amit Sarkar[2‡], Alok K. Sinha[2], Anoop S. Mahajan[3], Racheal Chacko[2], P. Sabu[2], Rajdeep Roy[4], Tim D. Jickells[5], David Stevens[6], Martin Wadley[6], Lucy J. Carpenter[1]

1. Wolfson Atmospheric Chemistry Laboratories, Department of Chemistry, University of York, York, YO10 5DD, UK.
2. National Centre for Polar and Ocean Research, Ministry of Earth Sciences, Goa 403804, India.
3. Indian Institute of Tropical Meteorology, Ministry of Earth Sciences, Pune 411008, India.
4. National Remote Sensing centre (NRSC), Indian Space Research Organisation (ISRO), Department of Space, Government of India.
5. Centre for Ocean and Atmospheric Sciences, School of Environmental Sciences, University of East Anglia, Norwich Research Park, Norwich, NR4 7TJ, UK.
6. Centre for Ocean and Atmospheric Sciences, School of Mathematics, University of East Anglia, Norwich Research Park, Norwich, NR4 7TJ, UK.

+ Authors contributed equally to this manuscript

Current address:
‡ Ecosystem based management of marine resources, (EBMMR), Environment and Life Sciences Research Center, Kuwait Institute for Scientific Research, Salmiya, Kuwait

* Correspondence: Corresponding author rosie.chance@york.ac.uk

Key words: iodine, iodide, iodate, seawater, Indian Ocean, Southern Ocean

Contribution to the Field

The presence of iodide-iodine at the ocean surface impacts air quality and climate. Specifically, the reaction of iodide with ozone at the sea surface is the dominant source of iodine to the atmosphere, and a significant sink for tropospheric (pollutant) ozone. In the atmosphere, iodine takes part in further reactions which remove more ozone, affect greenhouse gas lifetimes and contribute to particle formation. The rate of ozone removal and iodine emission depends on the sea surface iodide concentration, but iodide measurements are sparse and have hitherto been almost completely lacking in the Indian Ocean basin. Here we present an extensive new set of sea-surface iodide measurements, spanning latitudes from ~12°N to ~70°S and including measurements from the Bay of Bengal, the Arabian Sea, the open Indian Ocean and the Indian Ocean sector of the Southern Ocean. This data set represents a substantial increase in the global coverage of sea surface iodide observations. It will help improve our understanding of marine iodine biogeochemistry, and our ability to predict the impact of iodine chemistry on the atmosphere. We compare the observed distribution to that in other ocean basins, and explore the drivers of the distribution using an ocean iodine cycling model.

Abstract

Marine iodine speciation has emerged as a potential tracer of primary productivity, sedimentary inputs, and ocean oxygenation. The reaction of iodide with ozone at the sea surface has also been identified as the largest deposition sink for tropospheric ozone and is also thought to be the dominant source of iodine to the atmosphere. Accurate incorporation of these processes into atmospheric models requires improved understanding of iodide concentrations at the air-sea interface. Observations of sea surface iodide are relatively sparse and are particularly lacking in the Indian Ocean basin. We present 127 new sea surface (≤10 m depth) iodide and iodate observations made during three cruises in the Indian Ocean and the Indian sector of the Southern Ocean. The observations span latitudes from ~12°N to ~70°S, and include three distinct hydrographic regimes: the South Indian subtropical gyre, the Southern Ocean and the northern Indian Ocean including the Southern Bay of Bengal. Concentrations were broadly comparable to those observed at similar latitudes in other ocean basins. The spatial distribution of sea surface iodide follows the same general trends as in other ocean basins, with iodide concentrations tending to decrease with increasing latitude (and decreasing sea surface temperature). However, the gradient of this relationship was steeper in subtropical waters of the Indian Ocean than in the Atlantic or Pacific, suggesting that it might not be accurately represented by widely used parameterisations based on sea surface temperature. Iodide concentrations in the tropical northern Indian Ocean were higher and more variable than elsewhere. Two extremely high iodide concentrations (1241 and 949 nM) were encountered in the Bay of Bengal and are thought to be associated with sedimentary inputs under low oxygen conditions. Excluding these outliers, sea surface iodide concentrations ranged from 20 to 250 nM, with a median of 61 nM. Controls on sea surface iodide concentrations in the Indian Ocean were investigated using a state-of-the-art iodine cycling model. Multiple interacting factors were found to drive the iodide distribution. Dilution via vertical mixing and mixed layer depth shoaling are key controls, and both also modulate the impact of biogeochemical iodide formation and loss processes.

Introduction

Iodine is naturally present in the ocean, predominantly as the inorganic ions iodide (I^-) and iodate (IO_3^-). Iodine speciation is linked to many aspects of ocean biogeochemistry, and has been proposed as a tracer of primary productivity (Ducklow et al. 2018; Wong 2001), sedimentary inputs and oxygen status (Lu et al. 2018; Moriyasu et al. 2020). In addition, the concentration of iodide at the sea surface has recently attracted renewed interest from atmospheric chemists because of its impact on atmospheric composition and air quality e.g. (Sherwen et al. 2017; Cuevas et al. 2018). Specifically, the heterogeneous reaction of iodide with ozone at the sea surface has been identified as the largest, but also most uncertain, deposition sink for tropospheric ozone (Hardacre, Wild, and Emberson 2015), and the dominant source of volatile reactive iodine (as I_2 and HOI) to the lower atmosphere (Carpenter et al. 2013). Following emission from the ocean, reactive iodine species initiate catalytic ozone depletion cycles, and hence further influence the oxidative capacity of the atmosphere. Atmospheric iodine cycling results in the formation of iodide oxides, which have been implicated in the nucleation of particles in coastal marine areas (McFiggans et al. 2004; Allan et al. 2015).In remote marine locations, iodine chemistry may also indirectly contribute to the depletion of inorganic volatile species such as gaseous elemental mercury during the polar spring (Wang et al. 2014). The ozone-iodide reaction is now thought to be the dominant source of iodine to the atmosphere, with other sources (e.g. release of iodinated organic compounds by marine algae) contributing only around 20% of the total iodine flux to the atmosphere globally (Carpenter et al. 2013; Prados-Roman et al. 2015). To incorporate the sea surface ozone sink and/or iodine source into atmospheric models, iodide concentrations at the interface need to be predicted accurately. However, parameterizations for global sea surface iodide concentrations (MacDonald et al. 2014; Chance et al. 2014) have been limited by the relative scarcity of observations. This is particularly the case for the Indian Ocean basin, where only a few sea surface iodide observations have hitherto been reported (Chance et al. 2014), but atmospheric iodine chemistry has been investigated (e.g. (Mahajan et al. 2019).

In ocean waters, total inorganic iodine concentrations (the sum of iodide and iodate) behave approximately conservatively, with a value of around 450-500 nM across most of the oceans e.g. (Elderfield and Truesdale 1980; Truesdale, Bale, and Woodward 2000). Iodate is thermodynamically the more stable form under oxygenated conditions, and hence is present at higher concentrations throughout most ocean depths. However, at the ocean surface iodide concentrations are elevated and iodate depleted, despite this being thermodynamically unfavourable. Sea surface iodide concentrations typically range from undetectable to ~250 nM, with values higher than this only encountered as outliers (Chance et al. 2014). Iodide concentrations and the iodide to iodate ratio decline with depth below the euphotic zone, and iodide concentrations are generally very low (<20 nM) in oxygenated waters below ~500 m e.g.(Waite, Truesdale, and Olafsson 2006; Nakayama et al. 1989; Bluhm et al. 2011). The ratio of iodide to iodate varies with location as well as depth. Sea surface iodide concentrations exhibit a pronounced latitudinal gradient, with highest surface iodide concentrations observed at low latitudes and in coastal waters (Chance et al. 2014). In addition to these two inorganic forms, iodine also occurs in seawater associated with dissolved organic matter as so-called dissolved organic iodine (DOI; e.g. (Wong and Cheng 1998)). Organic forms of iodine are abundant in estuarine environments, where they can represent up to 64% of the total iodine (Wong and Cheng 1998; Schwehr and Santschi 2003). In the open ocean, levels of DOI are typically low (<5 % of the total iodine), but higher levels (e.g. 22% of total iodine) have sometimes been encountered (Wong and Cheng 1998).

The distribution of iodine species in the oceans is thought to result from a combination of hydrodynamic and biogeochemical drivers, which are not yet fully understood (Chance et al. 2014). The formation of iodide from iodate in the euphotic zone is thought to be associated with primary productivity, but the exact mechanism by which this occurs is not yet known (Chance et al. 2010; Campos et al. 1996; Bluhm et al. 2010). Similarly, the route for iodide oxidation back to iodate has been elusive, although recent work has suggested it may be linked to bacterial nitrification (Zic, Caric, and Ciglenecki 2013; Hughes et al. 2020). The lifetime of iodide with respect to oxidation is poorly constrained but thought to be relatively long, with estimates ranging from several months (Campos et al. 1996; Zic, Caric, and Ciglenecki 2013) or more (Hardisty et al. 2020), to as much as 40 years (Tsunogai 1971; Edwards and Truesdale 1997). Given the relatively long lifetime of iodide in seawater, its distribution is also strongly influenced by advection and vertical mixing e.g. (Campos et al. 1996; Truesdale, Bale, and Woodward 2000). The interplay of these driving factors results in global scale correlations between sea-surface iodide concentrations and sea-surface temperature (SST), and nitrate (Chance et al. 2014), which have been used to predict sea-surface iodide fields e.g. (Ganzeveld et al. 2009; MacDonald et al. 2014; Sarwar et al. 2016). In particular, spatial variations in ocean mixed layer depth are likely to be the primary cause of the widely used relationship between sea surface iodide concentration and SST.

This manuscript explores an extensive new set of sea surface iodide and iodate observations from the Indian Ocean and the Indian sector of the Southern Ocean, spanning latitudes from ~12°N to ~70°S, regions which until now have been lacking in observations (Chance et al. 2014). To the best of our knowledge, only three studies have previously reported iodine speciation in the Indian Ocean, and all have been in the west of the basin (East African coastal area (Truesdale 1978) and Arabian Sea (Farrenkopf and Luther 2002; Farrenkopf et al. 1997)). Of the data presented in these studies, there were only two sea surface iodide observations - both from the Arabian Sea (see Figure 1) - that could be included in Chance et al., 2014. The aim of this study was to substantially increase the number of observations in this region, in order to both improve understanding of large-scale gradients in ocean iodine speciation, and to increase global data coverage for model validation and the improvement of ocean iodide parameterisations. All of these will contribute to the creation of more accurate boundary conditions for atmospheric chemistry models.

Materials and methods

Sample collection

[Figure 1]

Samples were collected during three research cruises in the Indian Ocean and Indian sector of the Southern Ocean. Sampling locations for each cruise are shown in Figure 1. Samples were collected from the Bay of Bengal (BoB) during a zonal section cruise (Bay of Bengal Boundary Layer Experiment - BoBBLe) along 8°N, from 85.3°E to 89°E. The cruise took place between 24/6/2016 and 23/7/2016, on board the RV *Sindhu Sadhana*. In the Arabian Sea, samples were collected during the Rama mooring equatorial cruise IO1-16-SK (known as SK333 here), operated by Ministry of Earth Sciences, India (MoES) and National Oceanic and Atmospheric Administration, USA (NOAA), and taking place on the ORV *Sagar Kanya*. The cruise departed Chennai, India, on 23/08/2016 and returned to Sri Lanka on 23/09/2016. Samples were collected from the Southern Indian Ocean and Southern Ocean during the 9th

Indian Southern Ocean Expedition (SOE9; Jan-March 2017), from Mauritius (22°S) to coastal waters of Prydz Bay, Antarctica (69°S) on board the MV *SA Agulhas*. Sampling included both (Antarctic) coastal and open ocean waters during this cruise.

During the BoBBLe and SOE9 cruises, surface water samples were obtained manually from the upper 30-70 cm of the sea surface using a metal bucket deployed over the side of the ship near the stern. Additional depth profile samples were obtained using a CTD (911 plus, Sea-Bird Electronics, USA) rosette equipped with 12 Niskin bottles. During the SOE9 cruise, depth profiles were taken at 17 CTD stations, and additional surface samples were taken (by bucket) at least twice a day along the entire cruise track (except when the ship was stationary for CTD stations). Sampling included two time-series, one at ~40°S, and one in coastal Antarctic waters at ~68°S (around the Polar Front), during which samples were collected at 4 or 6 hour intervals for up to 72 hours. During the SK333 cruise, samples were only collected using a CTD rosette. Sample dates, times and locations for all cruises are given in the online dataset available from the British Oceanographic Data Centre (http://doi.org/czhx). In this manuscript, both shallow CTD samples (depth ≤ 10 m) and 'bucket' samples will be considered to be comparable, and representative of the ocean surface. This follows the approach taken in previous examinations of sea surface iodide concentrations (Chance et al. 2014). Note only surface samples are considered in this manuscript, although selected depth profiles are presented in the Supplementary information to aid interpretation of surface concentrations.

Immediately following collection, samples were filtered (Whatman GF/F) under gentle vacuum, and transferred to 50 mL polypropylene screw cap tubes. Duplicate aliquots were prepared for each sample. Aliquots were either stored at 4° C for on-board iodide determination within 24 hours, or frozen at -20° C for transport back to our laboratories for analysis. Analysis of frozen samples took place within 18 months of collection. Inorganic iodine speciation is preserved in frozen samples (≤-16° C) for at least one year (Campos 1997). To avoid possible contamination, sample bottles for the iodine samples were kept strictly separated from the dissolved oxygen reagents containing iodine.

Iodide and iodate analysis

Iodide was determined by cathodic stripping square wave voltammetry (Campos 1997; Luther, Swartz, and Ullman 1988) using a μAutolab III potentiostat connected to a 665VA stand (Metrohm) with a hanging mercury drop electrode, an Ag/AgCl reference electrode and a carbon or platinum auxiliary electrode. 12 (or 15) mL of the sample was introduced to a glass cell and 90 (or 112) μL of Triton X-100 (0.2%) was added. The sample was purged with N_2 (oxygen free grade) for 5 minutes before each measurement. The deposition potential was set at 0 V and deposition times were typically 60 s; scans ranged from 0 to -0.7 V, with a step of 2 mV, a 75 Hz frequency and a 0.02 V wave amplitude. Each scan was repeated 5-6 times, with scan repeatability equal or better than 5%. Calibration was by 2 or 3 standard additions of a KI solution (~10^{-5} or 10^{-6} M). Precision was estimated by repeat analysis (n = 6) of selected seawater samples over period of ten days and was found to be lower than 7% relative standard deviation.

Iodate was measured using a spectrophotometer (UV-1800, Shimadzu; 4 decimal places) after reduction to iodonium (I_3^-) (Jickells, Boyd, and Knap 1988; Truesdale and Spencer 1974). 2.3 mL of the sample was introduced in the 1 cm UV quartz cell, 50uL of sulfamic acid (1.5 M) was added, and the first absorbance value was obtained after 1 minute. Then 150 μL of KI (0.6 M) was added and the second absorbance read after 2.5 minutes. Iodate

concentrations were calculated from the difference between the two absorbances. Calibration was performed daily using a series of KIO_3 standard solutions. Samples were measured at least in triplicate with repeatability better than 5%; reported values are means. Reported errors are calculated by propagation of the standard deviation on the repeated measurements, the errors on the fit of the calibration and error on the volumes pipetted. Note that strictly, this method measures all inorganic iodine in oxidation states from 0 to +5, but as this fraction is dominated by iodate it is taken as a measure of iodate.

Supporting measurements

Samples from CTD stations use the temperature, salinity and depth data directly obtained from the CTD. Precision of these measurements was as follows: temperature: ± 0.001 °C; conductivity: ± 0.0001 S m^{-1}; depth: ± 0.005% of the full scale. CTD salinity was calibrated using a high-precision salinometer (Guildline AUTOSAL). Temperature and salinity of manually collected 'bucket' samples were determined using an outboard thermometer, and the salinometer respectively.

Samples for nitrate (NO_3^-) analysis were collected in 250 mL narrow mouth polypropylene amber bottles (Nalgene). Each bottle was rinsed twice with the sample water prior to collection. Analysis was performed onboard as soon as possible after sample collection, using an SKALAR SAN+ segmented continuous flow autoanalyzer. Precision and accuracy of NO_3^- measurements were ±0.06 and ±0.07 μM, respectively.

Ocean Modelling

The ocean iodine cycling model described in Wadley et al. (Wadley et al. 2020) was used to evaluate which physical and biogeochemical processes drive the observed trends in iodide concentration in the Indian Ocean and Indian sector of the Southern Ocean. The model comprises a biogeochemical model of iodine cycling embedded in a three-dimensional global ocean circulation framework, and has been calibrated using the data from a recently available extended global sea surface iodide compilation (Chance, Tinel, Sherwen, Baker, Bell, Brindle, Campos, Croot, Ducklow, He, Hopkins, et al. 2019) which includes the current data set, plus additional depth resolved iodide measurements (see (Wadley et al. 2020) for details). In the model, iodide production is driven by primary production, and iodide loss (by oxidation) is linked to biological nitrification. A spatially variable I:C ratio is used to allow the model to better capture the observed iodide concentrations.

Results and Discussion

Overview – Global scale trends

In total, 127 new sea surface iodide observations and 130 sea surface iodate observations are reported here for the three cruises, including two time series. Measurements were made at 98 different sampling locations, spanning latitudes from ~12°N to ~70°S. This is a substantial increase in data coverage for the Indian Ocean and the Indian sector of the Southern Ocean region, which was previously particularly lacking in observations of sea surface iodine speciation (Chance et al. 2014). As noted in the introduction, only two sea surface iodide observations for the Indian Ocean were included in Chance et al., 2014, and both were from the Arabian Sea (see Figure 1).

[Figure 2]

[Figure 3]

The highest iodide concentrations were observed in and approaching the tropics, while lower concentrations were observed at high latitudes (Figure 2). This latitudinal trend in sea surface iodide concentration broadly follows those observed in other ocean basins (Figure 3). In addition, a 'dip' in sea surface iodide concentrations is seen around the equator and elevated concentrations are seen in coastal polar waters, as observed elsewhere (Figures 2 & 3) (Chance et al. 2014; Chance et al. 2010). While these global scale trends are well documented in the Atlantic and Pacific basins e.g.(Bluhm et al. 2011; Campos, Sanders, and Jickells 1999; Truesdale, Bale, and Woodward 2000; Tsunogai and Henmi 1971), to the best of our knowledge this is the first time they have been confirmed in the Indian Ocean and the Indian section of the Southern Ocean.

[Figure 4]

Considering the entire data set (n=127), sea surface iodide concentrations ranged from 20 to 1241 nM, with a median of 61 nM (Figure 4). The very large range in the data is primarily due to the presence of two very high outliers in the Bay of Bengal, which are discussed later (Section 3.3). When these outliers are excluded, the upper limit of the data is reduced to 250 nM, bringing the range within the global range of marine iodide concentrations previously reported (Chance et al. 2014). The large range in the overall data set can mainly be ascribed to the large span of latitudes covered. The median value is somewhat lower than the global median value (77 nM; (Chance et al. 2014), reflecting the bias towards high latitude/low iodide samples in our data set.

[Figure 5]

Sea surface iodate concentrations ranged from 51 to 495 nM, with a median of 294 nM. Iodate concentrations broadly showed the opposite pattern to iodide concentrations, with highest median values in the Southern Ocean (median of 323 nM), intermediate values in the subtropical Indian Ocean (median of 294 nM) and lowest values in the tropical Indian Ocean (median 196 nM). However, there was only a very weak, inverse linear relationship between sea surface iodide and iodate concentrations ($R^2 = 0.16$, $p = 3 \times 10^{-6}$; Figure 5). Total iodine concentrations in seawater are typically ~450 nM ((Chance et al. 2014) and references therein), with the budget dominated by iodide and iodate. Here we find the sum of iodide and iodate was less than this at most sampling locations (Figure 5), with a median value of 380 nM (range 88 to 560 nM). Although somewhat unusual, comparable low total inorganic iodine concentrations have been reported elsewhere (e.g. North Sea (Hou et al. 2007), South East China Sea (Wong and Zhang 2003)). Depleted total inorganic iodine may be due to the uptake of iodine to the particulate phase in the surface ocean, or to the presence of a significant dissolved organic iodine reservoir. Although it could imply substantial loss of iodine from the surface ocean to the atmosphere, current knowledge suggests the magnitude of such fluxes (e.g. (Carpenter et al. 2013)) is too small to have such a large impact on the sea surface concentrations. No clear relationships were evident between total inorganic iodine and either latitude or nitrate concentration.

Our sampling area spanned a wide range of different water masses and biogeochemical conditions (Figure 2). Low temperature waters at high latitudes were characterised by high nitrate and low iodide concentrations, while further north in the subtropical gyre, nitrate concentrations were very low and iodide concentrations rose in step with decreasing latitude and increasing SST (Figure 2). North of the equator, SST becomes a poor predictor of iodide

concentration. To explore our data set further, we consider iodine speciation separately in each of three different hydrographic regimes (tropical, mid-latitudes and polar).

South Indian subtropical gyre (~23-42 °S)

Samples were collected from the southern Indian Ocean (~23-42 °S) during the SOE9 cruise. The samples form an approximate latitudinal transect along 57°E, encompassing the Indian South subtropical gyre and the subtropical convergence zone. All are open ocean. North of this region, the Southern Equatorial Current (SEC; not sampled in this work) has been noted as a clear biogeochemical front, separating subtropical gyre waters from the lower oxygen northern Indian Ocean (Grand et al. 2015). The subtropical gyre waters are characterised by very low nitrate concentrations and relatively high salinity (Figure 2), with SST rising from ~15°C in the south to ~29°C in the north.

Between these latitudes, iodide concentrations ranged from 35 to 235 nM and increased in an approximately linear manner with decreasing latitude. In this region, iodide is strongly correlated with both latitude ($R^2 = 0.86$, $p = 3 \times 10^{-20}$) and SST ($R^2_{adj} = 0.89$, $p = 2 \times 10^{-22}$). These are stronger correlations than the global relationships reported in Chance et al., 2014, and also have steeper gradients (Table 1). Using the extended dataset of global sea surface iodide observations (Chance et al., 2019), sea surface iodide gradients in each of the ocean basins were compared. Considering each of the major ocean gyres individually reveals that the latitudinal dependency of iodide is greater in the Indian Ocean than in the north Atlantic, north Pacific, south Pacific (excluding observations from the Peruvian upwelling, which do not conform to a linear latitudinal trend) or south Atlantic (Figure 3; Supp Info Table 1). This trend is driven by concentrations at the northern limit of our Indian Ocean observations (~25°S) being approximately double those at comparable latitudes in the other ocean basins, rather than a difference between concentrations at the poleward limit (Figure 3).

The same trend is also evident when the relationships between iodide and SST are considered. Although SST is not thought to directly impact iodine cycling itself, this relationship is important as it is widely used to predict sea surface iodide concentration fields for use in atmospheric models (e.g. (Sarwar et al. 2016)). The observed iodide vs. SST gradient is steeper in the Indian Ocean than other basins (Supp Info Table 1), implying the differences between basins cannot entirely be accounted for by differences in SST gradients. In any case, examination of climatological data (World Ocean Atlas, see Chance et al., 2014 for details) for the locations and months of iodide observations does not demonstrate any clear differences in SST, nitrate or mixed layer depth (MLD; defined using potential temperature) between ocean basins that might account for the difference in iodide gradient. This is explored further in Section 4.2. As a result, the stronger latitudinal dependency of iodide in the Indian Ocean that we observe here is not replicated in sea surface iodide values predicted using commonly employed parametrisations based on sea surface temperature (Chance et al. 2014; MacDonald et al. 2014). This is likely to introduce uncertainties specific to the Indian Ocean when using such parameterisations, for example in model calculations of iodine emissions from the sea surface.

The observational data is too limited to properly evaluate whether the pattern is the result of seasonal biases in sampling; all subtropical Indian Ocean observations were made during the southern hemisphere summer (January and February), while the modal months for observations in other basins were November (North Atlantic and South Pacific), October (South Atlantic) and March (North Pacific), see table S1. In the South Pacific, 90% of observations were made in January, i.e. in the same season as the Indian Ocean data. Despite

this, they have a lower latitudinal gradient (m = 2.8 compared to 9.5; table S1), hinting that the difference between basins is not due to seasonal variation and/or sampling biases and may instead be due to differences in iodine cycling.

With the exception of one higher value of 1.45 μM, observed sea surface nitrate concentrations in this region were generally low, with 86% of data points being below 0.5 μM. No relationship between nitrate and iodide was apparent (R^2 = 0.0004; Table 1), implying sea surface nitrate concentrations are a poor predictor of sea surface iodide in this hydrographic region. This likely reflects the fact nitrate concentrations were all very low, while substantial gradients in iodide concentrations were present. Campos et al. (Campos, Sanders, and Jickells 1999) have previously reported significant relationships between iodide and nitrate in the subtropical Atlantic, but as these were based on measurements from the upper 100 m of the water column rather than just the surface, and encompassed a range of nitrate concentrations, they are not directly comparable.

[Table 1]

Southern Ocean domain (~42˚S - 68˚S)

At the subtropical front around 42˚ S, a decrease in salinity is accompanied by a sharp increase in nitrate concentration (Figure 2). This front marks the transition from the Indian Ocean to the Southern Ocean (Orsi, Whitworth, and Nowlin 1995). The colder, nutrient rich waters south of the subtropical front have much lower iodide content, with a median concentration of 43 nM and range of 20 to 104 nM (Figure 4). Relationships between iodide concentrations and latitude or SST are much weaker than those observed further north (Table 1). This may be due to disruption by strong, but variable, vertical mixing events, which are characteristic of the Southern Ocean. No significant relationship between sea surface iodide and nitrate was observed in the Southern Ocean samples (Table 1). Negative correlations between iodide and nitrate have previously been reported for the upper 500 m of the water column in the Atlantic sector of the Southern Ocean, including the Weddell Sea (Campos, Sanders, and Jickells 1999), but were not replicated in a later study in the same area (Bluhm et al. 2011). At an Antarctic coastal site, only weak negative correlations between iodide and nitrate concentrations were observed (Chance et al. 2010).

The Southern Ocean samples may be further subdivided into coastal (i.e. near the Antarctic continent) and open ocean samples. The former category was defined as samples falling within the Austral Polar biogeochemical province (Longhurst 1998), while the latter category included samples from both the Antarctic and Sub-Antarctic provinces, and spanned the Polar Front. The range and distribution of concentrations seen in the coastal and open ocean subsets are very similar (Figure 4), despite the coastal samples spanning a much narrower latitudinal range (69 - 64° S, compared to 63 - 43° S). In the open ocean sub-set, iodide concentrations generally decrease moving south (R^2 = 0.16; p = 0.04), while in the coastal samples at the most southerly extreme of the data set, this relationship breaks down (R^2 = 0.02; Figure 2). A similar pattern is also reported in the global compilation of Chance et al. (2014), where Southern Ocean and Antarctic samples were predominantly from the Atlantic sector and the western Antarctic Peninsula. The range of concentrations observed in the Antarctic coastal samples (20 to 95 nM) is within that observed previously in coastal Antarctic waters during the austral summer (Chance et al. 2010). The magnitude of this variability is greater than can

be accounted for by normalizing the iodide concentrations to salinity variations (e.g. due to ice melt water).

Northern Indian Ocean including southern Bay of Bengal (~4° S - 11° N)

Samples were collected from tropical waters in the northern Indian Ocean during the BoBBLe (Bay of Bengal) and SK333 (Arabian Sea) cruises. The latitudinal range of this sample sub-set was ~4° S to ~11° N, and all were considered to be open ocean. These sampling locations were within the Indian Monsoon Gyre biogeochemical province, and shared high sea-surface temperatures, variable salinity and typically low nitrate concentrations. This sample sub-set showed the highest, and most variable iodide concentrations (range 63 to 1241 nM, median 165 nM; Figure 4). This was primarily due to the occurrence of two extremely high iodide concentrations (>900 nM) in the Bay of Bengal; excluding these values, the range in tropical open ocean iodide was still the largest of the three hydrographic regions surveyed, with a maximum of 250 nM being observed in the Bay of Bengal (Figure 4). Such concentrations are comparable to measurements made at similar latitudes elsewhere (Figure 3).

All but one of the samples collected around the equator (~5°S to ~3°N) during the SK333 cruise had iodide concentrations in the range ~80 to 120 nM. The exception to this was at 67°E, 0°N (CTD2), where iodide concentrations reached ~200 nM. As iodide concentrations were typically lower than in tropical waters further north and south (Figure 2), there was a positive rather than negative correlation between iodide and absolute latitude in this sample set (Table 1). A similar dip at very low latitudes is also seen in the Atlantic and Pacific (Figure 3; Chance et al., 2014). This feature is replicated in our model and is thought to be due to equatorial upwelling (see Section 4).

As already noted, exceptionally high sea surface iodide concentrations of 1241 and 949 nM were observed at two stations in the Bay of Bengal (UWI BS3 & UWI BS8). Very high near-surface iodide concentrations were also observed at Station AR nearby (2039, 1546 & 479 nM at 10, 25 & 50 m respectively; see Figure S1 in Supplementary Information). We believe these concentrations are real, and not the result of contamination or analytical error because: (i) repeat analyses gave the same results, (ii) very high concentration samples were also analysed by ion chromatography, a completely independent method, and this yielded concentrations within 10% of those obtained by voltammetry (1277 and 960 nM for samples BS3 and BS8 respectively, and 1693 nM for Station AR at 25 m depth), (iii) results for station AR show oceanographic consistency (see Figure S1), (iv) no likely sources of iodine contamination were present during sampling. It is possible that the high, very localised, iodide concentrations could arise from the break-down of an iodine rich substrate, for instance a mass of brown macroalgae such as Laminaria digitata. However, nothing unusual of this nature was observed during sampling. These very high iodide levels result in total (dissolved) inorganic iodine concentrations several times higher than the near universally observed value of ~500 nM (Chance et al. 2014). They cannot be accounted for by the reduction of iodate, and instead imply an exogenous source of iodide-iodine.

Samples with elevated iodide exhibited relatively low surface salinity (Figure S1, Supp Info), possibly indicating an association with freshwater inputs. The Bay of Bengal is characterized by very heterogenous salinity - low salinity is caused by monsoon rainfall and high riverine inputs to the north, while high salinity water arrives from the Arabian Sea via the intense Southwest Monsoon Current (SMC). The BoBBLe cruise took place during the Asian summer monsoon season, during which the region experiences high rainfall. However,

atmospheric wet deposition is thought unlikely to be the source of elevated iodide because meteoric water has a lower iodine content than seawater (20-124 nM (Sadasivan and Anand 1979); 4.7-26.2 nM; (Gilfedder, Petri, and Biester 2007)). Furthermore, observations of elevated sea surface iodide did not correspond to rainfall events encountered during the BoBBLe cruise itself. Similarly, riverine inputs are unlikely to be the iodide source, as total iodine concentrations in rivers, including the Ganges, are lower than or comparable to those in seawater (≤ 20 ug/L, ~ 157 nM; (Moran, Oktay, and Santschi 2002; Ghose, Das, and Saha 2003)), and the area surveyed was away from major outflows. While freshwater inputs are thus not thought to be the source of the excess iodide, stratification caused by rainwater dilution of surface layers could perhaps contribute to the persistence of high iodide concentrations at the ocean surface.

In addition to the SMC, the second main oceanographic feature in the BoBBLe study area is a wind driven upwelling feature called the Sri Lanka Dome (SLD), which manifests as a large cyclonic gyre in the south western part of the BoB to the east of Sri Lanka. The SLD is identified as an area of negative mean sea level anomaly and a relatively shallow thermocline. Both the SLD and the SMC were well developed and distinct during the study period (Vinayachandran et al. 2018). Extreme iodide values were observed at stations north (AR, BS3) and east (BS8) of the SLD, but not in the stations that were inside the SLD (Figure S2, Supp Info) (Vinayachandran et al. 2018). High iodide station AR exhibited high seawater pCO_2 (467–554 atm), low surface pH and low alkalinity, indicative of upwelled waters that are presumed to be associated with the SMC (Vinayachandran et al. 2018). Station BS3 was close in space and time, while station BS8 was also influenced by the SMC (Vinayachandran et al. 2018). We therefore speculate that the high iodide observed is in some way related to the SMC. However, the high salinity core of the SMC (i.e. Arabian Sea water), which was evident at depths of ~25-150 m at stations east of the SLD, was not itself associated with elevated iodide (Figure S1, Supp Info). This suggests the excess iodide was not in the main water mass carried by the SMC, and did not originate from the Arabian Sea.

Comparable high iodide concentrations have previously been observed in low oxygen sub-surface waters in the north western part of the Arabian Sea (Farrenkopf and Luther 2002); these were attributed to advection from shelf sediments. More recently, plumes of very high iodide sub-surface concentrations (~1000 nM) have also been reported in sub-oxic waters in the Eastern Tropical South Pacific (ETSP) (Cutter et al. 2018) and the Eastern Tropical North Pacific (ETNP) (Moriyasu et al. 2020). In the ETSP, the plume followed an isopycnal and was associated with corresponding features in Fe(II) and nitrite, so was again thought to be due to a shelf sediment iodide source (Cutter et al. 2018). Elevated concentrations persisted more than 1000 km from the shelf break due to the relatively long iodide lifetime in seawater with respect to oxidation. Trace metal concentrations were not measured during the BoBBLe cruise, but sub-surface waters in the region have previously been reported to contain additional dissolved Fe from sedimentary inputs (Grand et al. 2015), suggesting it is plausible that stations on the edge of the SLD could be influenced by sedimentary interactions. Waters over the western Indian shelf experience severe hypoxia (Naqvi et al. 2000), and so could be subject to significant sedimentary iodide inputs as implicated in other low oxygen regions (Cutter et al. 2018; Farrenkopf and Luther 2002). During the Southwest Monsoon, the West Indian Coastal Current (WICC) flows south along the west coast of India, and these waters are advected along the path of the SMC into the BoB. We speculate that such waters have potential to contain 'excess' iodide levels as a result of sedimentary inputs, and that it is the remnants of these water masses that we may have sampled.

We believe this is the third reported observation of very elevated (>500 nM) iodide concentrations at the surface of the open ocean. The dataset reported by Cutter et al. (2018) contains two surface samples with iodide concentrations of 594 and 960 nM immediately off the coast of Peru, while transects in (Moriyasu et al. 2020), show patches of high iodide outcropping at the surface. An extreme surface iodide concentration of ~700 nM has also been reported for the brackish waters of the Skaggerrak (Truesdale, Danielssen, and Waite 2003), a shallow strait that is subject to hypoxia (Johannessen and Dahl 1996). The paucity of previous observations suggests it is a rare phenomenon, but it may nonetheless be of local significance. Atmospheric ozone deposition and iodine emission fluxes will proportionally increase where surface iodide concentrations are high. An increase in iodide from 150 to 2050 nM (x 13.7) leads to a 5-6 fold increase in total iodine emissions, for a typical ambient ozone concentration of 25 ppb and a wind speed of 7 m s^{-1} (Figure S3, Supp Info). This comprises a 4.5-fold increase in HOI emissions, which dominates the flux, and a 30-fold increase in I_2 emissions, which increase from 5.5% of the total flux at 150 nM iodide to 28% at 2050 nM iodide. It is assumed that the regional atmospheric impact of such 'hot-spots' will be low, as they will only represent a small proportion of the relevant footprint area. However, the atmospheric impacts of such areas may become significant if either very localised processes are being considered, or their extent and/or frequency of occurrence increases. As areas of low oxygen waters in contact with shelf sediments become more extensive (Naqvi et al. 2000), the possibility that this could impact on surface iodide concentrations in coastal regions may need to be considered. Understanding the potential impact of low oxygen conditions and sedimentary inputs on surface iodide concentrations, and hence local atmospheric chemistry, requires both the sedimentary fluxes and the lifetime of iodide in oxygenated seawater to be better constrained. The atmospheric boundary layer above the northern Indian Ocean has high iodine oxide (IO) levels, with inputs dominated by the inorganic iodine flux from the ozone-iodide reaction (>90%), as a result of "ozone-related" pollution outflow (Prados-Roman et al. 2015). Hence atmospheric chemistry in the region may be particularly sensitive to changes in the surface iodide budget.

Exploring controls on the sea surface iodide distribution in the Indian Ocean using an ocean iodine cycling model

The trends in sea surface iodide concentrations observed across the south Indian subtropical gyre and Indian sector of the Southern Ocean are well replicated by the iodine cycling model of Wadley et al. (Wadley et al. 2020) (Figure 6a). In the northern Indian Ocean agreement between model and observations is poorer, but modelled concentrations fall within the range of the observations in the area. Furthermore, the model predicts unusually high iodide concentrations in the BoB, where extremely high iodide concentrations were observed. Note the model does not currently include sedimentary processes, so this suggests that additional physical and biogeochemical processes may also contribute to elevated iodide levels in the BoB. Given the generally good agreement between observed and modelled iodide concentrations, we explored the controls on the iodide distribution in the study area by examining the physical and biogeochemical drivers of iodine cycling within the model.

The influence of physical and biogeochemical processes on the iodide distribution

The sea surface iodide distribution is thought to result from the interplay of biological formation and loss processes, and physical mixing and transport (Chance et al., 2014), and these processes are represented in the iodine cycling model (Wadley et al. 2020). Biological productivity drives iodide formation in the model, but direct associations between the spatial distribution of productivity and iodide (either observed or simulated) are not seen in the

Indian Ocean basin (Figure 6a, b). Most notably, the strong peak in productivity centred on 40°S (Figure 6b) has no corresponding peak in either observed or simulated iodide concentrations. This indicates that other processes are also important in determining the iodide distribution. Imposing a constant level of productivity (set at the annual mean for each grid point) throughout the year had very little effect on modelled iodide concentrations, (Figure 6c), suggesting that the relationship between the seasonal cycle of iodide production and physical factors (e.g. MLD, see below) does not have a significant effect on iodide concentrations. Halving the productivity in the model reduces simulated iodide concentrations by around a half south of 40°S (where iodide is very low, and iodate high), but only by around a quarter north of 40°S, and has almost no effect in the northern Indian Ocean where modelled iodide is highest (and thus modelled iodate lowest, at ≤ 300 nM). This may indicate that lower iodate concentrations to the north limit iodide production. The amount of iodide produced per unit primary productivity is specified in a spatially variable I:C ratio (Figure 6e; (Wadley et al. 2020). Halving this ratio is equivalent to halving primary production, and has identical consequences (Figure 6f).

Iodide produced by primary productivity is distributed throughout the mixed layer, and surface concentrations are therefore dependent on the MLD. Summer MLD minima are similar throughout the section, with typical values of a few tens of metres, whereas late winter MLD maxima increase with latitude (Figure 6j).
Deepening of the MLD decreases iodide concentrations throughout the mixed layer as a result of dilution, while shoaling of the MLD decreases the total amount of iodine present integrated over the mixed layer, but does not change the concentration at any given depth within it. Removing the seasonal cycle of MLD in the model (by replacing with the annual mean MLD for each grid point) increases surface iodide concentrations, particularly at lower latitudes (Figure 6k), indicating that the removal of iodide through MLD shoaling is important. Removing both seasonal and spatial variation in the MLD by setting it to a uniform 56 m results in substantial increases in surface iodide concentrations at higher latitudes (Figure 6l), due to elimination of both dilution and shoaling effects. In contrast, doubling the MLD decreases iodide concentrations, with the greatest effect seen where iodide concentrations are highest (Figure 6m). Interestingly, this brings modelled and observed iodide concentrations into good agreement around the equator. Inspection of SK333 CTD data indicates that at the time of sampling, actual MLDs in this region (between 50 to 100 m) were deeper than the climatological values used in the model (less than 40 m; Figure 6j), which may indicate that short term variations in MLD, for example due to weather events, affected iodide concentrations. In the model, the release of iodide from phytoplankton occurs 60 days after the uptake of carbon, and the interplay of this lag period with the MLD cycle could influence iodide concentrations. However, changing the duration of the lag to 0 and 120 days in the model has only a small impact on the iodide, and only at high latitudes (Figures 6g and 6h).

The seasonal MLD cycle imposes an annual timescale on the removal of iodide from the mixed layer where the seasonal cycle has a large amplitude, but vertical and horizontal advection also exchange water between the surface layer and ocean interior. Turning off the circulation in the model, so that vertical mixing is the only physical mechanism for iodide removal from the mixed layer also results in increased mixed layer iodide concentrations at almost all locations (Figure 6n), In addition to removal by MLD shoaling, the model also allows for the removal of mixed layer iodide by oxidation to iodate, via a pathway linked to nitrification ((Hughes et al. 2020; Wadley et al. 2020)). Eliminating this pathway has little impact on modelled iodide concentrations at high latitudes, but results in a significant

increase in concentrations north of 40°S (Figure 6i). This is because the iodide oxidation timescale in the model is multi-annual, and hence its impact is modulated by the lifetime of iodide in the mixed layer with reference to vertical mixing. At high latitudes, large seasonal changes in the MLD result in low sensitivity to oxidation, whereas at lower latitudes there is less annual mixed layer exchange, resulting in a longer iodide residence time, and hence oxidation is a more important process for mixed layer iodide removal.

The net surface fresh water flux resulting from precipitation and evaporation acts to respectively dilute or concentrate iodide in the mixed layer (Figure 6o). Setting the P-E flux to zero has a small impact on iodide, decreasing concentrations in the subtropical gyres where evaporation is strong. Thus at these latitudes evaporation results in a modest increase in iodide concentrations.

The model sensitivity tests described above confirm that sea surface iodide concentrations in the Indian and Southern Oceans are determined by a combination of factors which interact non-linearly. The dominant processes that determine iodide concentrations are the rate of iodide production, which is a function of productivity and the I:C ratio, and the MLD and its seasonal cycle, which acts to dilute and remove iodide from the surface layer. Loss by oxidation has the greatest impact at lower latitudes where physical removal mechanisms are weakest. As the climate changes over coming decades, changes in any of these factors are likely to result in changes in sea surface iodide concentrations. For example, the 100 to 300 m depth layer in the Indian Ocean has significantly warmed since 2003 as a result of heat distribution from the Pacific (Nieves et al., 2015) and this is likely to reduce stratification, and enhance vertical mixing, with an accompanying reduction in mixed layer iodide concentrations. Conversely, changes in nutrient inputs to the Indian Ocean and declining oxygen levels will act to reduce iodide oxidation, due to its association with nitrification (Hughes et al. 2020), and hence may act to increase iodide concentrations. Any changes in productivity, and/or shifts to different phytoplankton types with different I:C ratios, will also potentially alter the rate of iodide production, although this has been found to predominantly impact on iodide concentrations at higher latitudes (Wadley et al., *Manuscript In Preparation*).

[Figure 6]

Difference in latitudinal iodide gradients between the subtropical Indian and Atlantic Oceans

As described earlier, observed sea-surface iodide concentrations have a steeper latitudinal gradient (and related SST dependency) in the subtropical Indian Ocean than reported for other ocean basins (Supplementary Information, Table S1), and this may limit the accuracy of global scale parameterisations relating iodide to SST. Although less pronounced, this feature is replicated in the model output (see table S1), and therefore a series of sensitivity tests have been conducted to investigate which processes may be responsible for the apparent differences in the latitudinal iodide gradient between ocean basins. Specifically, the model was run with each of the iodide forcing processes in the Indian Ocean and Indian sector of the Southern Ocean replaced by those from the Atlantic. Figure 7 shows the forcing fields used for the two ocean basins, and the modelled iodide concentrations generated using these fields. The gradient of iodide against latitude is significantly increased between 30°S and 20°S when the Indian Ocean and Indian sector of the Southern Ocean productivity fields are replaced with values for the same latitudes in the Atlantic. This is driven by a smaller decrease in

productivity with decreasing latitude in the Indian Ocean than the Atlantic. Thus productivity differences act to decrease, rather than increase the iodide gradient. Removal of iodide from the mixed layer by oxidation occurs as a function of nitrification (Wadley et al. 2020), which is parameterised using the proportion of nitrate regenerated in the mixed layer (see Yool et al., 2007). Differences between this ratio in the subtropical regions of the Indian and Atlantic oceans are small (Figure 7d), and have negligible impact on the modelled iodide in the Indian Ocean (Figure 7e). At lower latitudes MLDs are similar in the two basins, but between ~35 and 45°S, MLDs are significantly deeper in the Atlantic due to the greater northward extent of polar waters (Figure 7f). Since a deeper MLD dilutes iodide, modelled iodide concentrations are lower between 45°S and 35°S with Atlantic MLDs imposed in the Indian basin (Figure 7g), and this increases the latitudinal gradient of iodide, contrary to the observed difference in gradients between the basins. Precipitation and evaporation act to dilute/concentrate iodide in the mixed layer, so changes in the net fresh water flux with latitude could influence the latitudinal iodide gradient. The model was run with the Atlantic surface fresh water flux imposed in the Indian Basin (Figure 7h). This was found to have a negligible effect on iodide (Figure 7i). Finally, the I:C ratio in the model determines the amount of iodide produced per unit carbon of primary production. This ratio is found to be greater (more iodide produced per unit carbon) in the Indian than Atlantic Ocean to allow the model to fit the observed iodide in each basin (Figure 7j). The I:C ratio in the Indian Ocean was replaced by that for the Atlantic Ocean in the model (Figure 7k). This results in decreased iodide production, and iodide concentrations, but the latitudinal gradient of iodide shows little overall change between 41°S and 23°S. It should be noted that the model does underestimate the iodide gradient in the Indian Ocean (See Table S1), and refinement of the spatial variation of the I:C ratio in the model to improve the model fit to observations is likely to show that it is the I:C ratio which is responsible for the greater observed latitudinal gradient of iodide in the model.

In summary, basin scale differences in the above four forcing fields investigated here (productivity, nitrification, MLD and P-E) do not appear to explain the difference in latitudinal iodide gradient between the subtropical Indian and southern Atlantic oceans. In fact, differences in productivity and MLD between the two basins would appear to have the opposite effect, with Atlantic forcing fields resulting in a steeper gradient than Indian Ocean forcing fields. The above analysis implies that the difference in sea-surface iodide concentration gradient between the Indian Ocean and the other ocean basins is not the result of geographical or seasonal differences in either physical mixing and/or ocean circulation, or primary production, as these features are accounted for by the model. Instead we suggest the difference may be the result of different phytoplankton types, with differing I:C iodide production ratios, in the two basins. A spatially variable I:C ratio is used in the model to allow the model to fit the global observations (Wadley et al. 2020), and across all latitudes this is higher for the Indian Ocean/Indian sector of the Southern Ocean than the Atlantic. The need for this I:C ratio adjustment implies that the difference might instead arise from differences in microbiological community composition, and/or the expression of metabolic processes by such organisms. *Synechococcus* dominates in the subtropical Indian Ocean, whereas Nanoeucaryotes and *Prochlorococcus* dominate in the subtropical Atlantic (Alvain et al., 2008). Recent work by our group indicates that the I:C ratio associated with iodide production varies between phytoplankton types, with *Synechococcus* having a higher I:C ratio than Nanoeucaryotes and *Prochlorococcus* types (Wadley et al., *Manuscript in Preparation*). Hence the higher relative abundance of *Synechococcus* in the subtropical Indian Ocean might account for the higher iodide concentrations observed at low latitudes, and the resulting steeper sea-surface iodide gradient. This also indicates that any change in

microbiological community composition associated with climate change could significantly impact ocean iodide concentrations.

[Figure 7]

Concluding remarks

This study has contributed 127 new sea surface iodide observations to the available measurements, which represents a substantial (>10%) increase in the number of available measurements (925 individual observations were included in Chance et al., 2014). The observations span nearly 80 degrees latitude in the Indian Ocean and Indian sector of the Southern Ocean, a region where very few (n=2) surface observations were previously available. Increased observations will facilitate better predictions of sea surface iodide concentrations, and consequent atmospheric chemistry, and this data has already been incorporated in a new global iodide parameterisation (Sherwen et al. 2019).

The large scale latitudinal trends observed in the Indian Ocean and Indian sector of the Southern Ocean are similar to those in other ocean basins (Chance et al. 2014). We have used a state-of-the-art global iodine cycling model (Wadley et al. 2020) to explore the controls on the sea-surface iodide distribution in the Indian Ocean basin. Model sensitivity tests indicate that sea surface iodide is likely to be a function of vertical mixing and the seasonal cycle in MLD, the rate of iodide production, which is related to productivity and the I:C ratio, and – at lower latitudes – iodide oxidation in the mixed layer. These factors interact in a non-linear manner.

At subtropical latitudes, the latitudinal and temperature dependency of iodide is steeper than in other ocean basins. Therefore, using global scale relationships with SST (e.g. (MacDonald et al. 2014)) to predict regional scale iodide concentrations for the Indian Ocean will be subject to biases. Exploration of this basin scale difference using the model indicates that it is driven by differences in biological productivity at subtropical latitudes.

Exceptionally high iodide concentrations were observed at a small number of stations in the northern Indian Ocean. Such high concentrations are rare, but have been reported previously in low oxygen subsurface waters (Farrenkopf and Luther 2002), and more recently, in surface waters above the Peruvian and Mexican oxygen deficient zones (Cutter et al. 2018; Moriyasu et al. 2020). In all cases, the excess iodide is suggested to be sedimentary in origin, raising the possibility that processes at the sea floor could influence air-sea interactions, should that water reach the sea surface. Although such iodide 'hot-spots' are unlikely to have significant impact on a global or regional scale, it is possible they may impact on local scale air-sea exchange processes involving iodine. Their existence also means care must be taken to ensure iodide concentrations used to generate parameterisations are representative of the entire study area.

Marine iodine cycling is anticipated to be affected by global change, with consequent impacts on atmospheric chemistry. The Indian Ocean basin is subject to a number of specific pressures with potential to affect iodine cycling. Despite the empirical relationship between SSI and SST, changes in vertical mixing as a result of the Indian Ocean warming may in fact reduce mixed layer iodide concentrations. Meanwhile, changes to biological processes as a result of anthropogenic nutrient inputs, ocean deoxygenation and changes in heat distribution

777 are likely to impact iodide production and loss processes. Such changes will in turn impact
778 ozone deposition and iodine emission from the sea surface.

Data Availability Statement

Sea surface iodide concentration data described in this work is available from the British Oceanographic Data Centre, as part of a global compilation of observations doi:10/czhx (Chance, Tinel, Sherwen, Baker, Bell, Brindle, Campos, Croot, Ducklow, He, Hopkins, et al. 2019; Chance, Tinel, Sherwen, Baker, Bell, Brindle, Campos, Croot, Ducklow, He, Hoogakker, et al. 2019). Additional supporting datasets are available on request to the corresponding author.

Author contributions

LT, AS, AKS and AM collected seawater samples during the three research cruises; LT and RJC analysed samples for iodine speciation; AS, AKS and RR provided supporting biogeochemical measurements; RC and PS provided insight regarding physical oceanography in the study area; DS and MW performed the iodine modelling described in Section 4; RJC and LT interpreted the data and wrote the manuscript with input from TDJ and MW, other authors also provided comments on the manuscript; LJC, TDJ, AM and RJC conceived the study.

Funding

This work was funded by UK NERC grants NE/N009983/1, and NE/N01054X/1, awarded to RJC, LT, TDJ, MW, DS and LJC. The research cruises were funded by the Ministry of Earth Sciences, India, and we thank the National Centre for Polar and Ocean Research for generously providing LT a berth on the ISOE-09 expedition.

Conflict of Interest

The authors declare no competing interests.

Acknowledgements

We are grateful to the officers, crew and scientific parties onboard MV *SA Agulhas*, ORV *Sagar Kanya* and RV *Sindhu Sadhana* for their essential support during the research cruises. We also thank Alex R. Baker (University of East Anglia) for loan of analytical equipment. The model simulations were undertaken on the High Performance Computing Cluster supported by the Research and Specialist Computing Support service at the University of East Anglia.

References

Aksenov, Yevgeny, Sheldon Bacon, Andrew C. Coward, and A. J. George Nurser. 2010. 'The North Atlantic inflow to the Arctic Ocean: High-resolution model study', Journal of Marine Systems, 79: 1-22.

Allan, J. D., P. I. Williams, J. Najera, J. D. Whitehead, M. J. Flynn, J. W. Taylor, D. Liu, E. Darbyshire, L. J. Carpenter, R. Chance, S. J. Andrews, S. C. Hackenberg, and G. McFiggans. 2015. 'Iodine observed in new particle formation events in the Arctic atmosphere during ACCACIA', Atmospheric Chemistry and Physics (Print), 15: 5599-609.

Behrenfeld, Michael, and Paul Falkowski. 1997. 'Behrenfeld MJ, Falkowski PG. Photosynthetic rates derived from satellite-based chlorophyll concentration. Limnol Oceanogr 41: 1-20', Limnology and Oceanography, 42: 1-20.

Bluhm, K., P. L. Croot, O. Huhn, G. Rohardt, and K. Lochte. 2011. 'Distribution of iodide and iodate in the Atlantic sector of the southern ocean during austral summer', Deep-Sea Research Part II-Topical Studies in Oceanography, 58: 2733-48.

Bluhm, K., P. Croot, K. Wuttig, and K. Lochte. 2010. 'Transformation of iodate to iodide in marine phytoplankton driven by cell senescence', Aquatic Biology, 11: 1-15.

Campos, M.L.A.M. 1997. 'New approach to evaluating dissolved iodine speciation in natural waters using cathodic stripping voltammetry and a storage study for preserving iodine species', Marine Chemistry, 57: 107-17.

Campos, M.L.A.M., A. M. Farrenkopf, T. D. Jickells, and G. W. Luther. 1996. 'A comparison of dissolved iodine cycling at the Bermuda Atlantic Time-Series station and Hawaii Ocean Time-Series Station', Deep-Sea Research Part II: Topical Studies in Oceanography, 43: 455-66.

Campos, M.L.A.M., R. Sanders, and T. Jickells. 1999. 'The dissolved iodate and iodide distribution in the South Atlantic from the Weddell Sea to Brazil', Marine Chemistry, 65: 167-75.

Carpenter, L. J., S. M. MacDonald, M. D. Shaw, R. Kumar, R. W. Saunders, R. Parthipan, J. Wilson, and J. M. C. Plane. 2013. 'Atmospheric iodine levels influenced by sea surface emissions of inorganic iodine', Nature Geoscience, 6: 108-11.

Chance, R., A. R. Baker, L. Carpenter, and T. D. Jickells. 2014. 'The distribution of iodide at the sea surface', Environmental Science-Processes & Impacts, 16: 1841-59.

Chance, R.J., L. Tinel, T. Sherwen, A. Baker, T. Bell, J. Brindle, M.L.A.M. Campos, P. Croot, H. Ducklow, P. He, B. Hoogakker, F.E. Hopkins, C. Hughes, T. Jickells, D. Loades, D.A. Reyes Macaya, A.S. Mahajan, G. Malin, D.P. Phillips, A.K. Sinha, A. Sarkar, I.J. Roberts, R. Roy, X. Song, H.A. Winklebauer, K. Wuttig, M. Yang, P. Zhou, and L.J. Carpenter. 2019. "Global sea-surface iodide observations, 1967-2018." In. British Oceanographic Data Centre - Natural Environment Research Council, UK.

Chance, R.J., L. Tinel, T. Sherwen, A.R. Baker, T. Bell, J. Brindle, M.L.A.M. Campos, P. Croot, H. Ducklow, P. He, F. Hopkins, B. Hoogakker, C. Hughes, T.D. Jickells, D. Loades, D.A.R. Macaya, A.S. Mahajan, G. Malin, D. Phillips, I. Roberts, R. Roy, A. Sarkar, A.K. Sinha, X. Song, H. Winkelbauer, K. Wuttig, M. Yang, Peng Zhou, and L.J. Carpenter. 2019. 'Global sea-surface iodide observations, 1967-2018', Scientific Data, 6: 286.

Chance, Rosie, Keith Weston, Alex R. Baker, Claire Hughes, Gill Malin, Lucy Carpenter, Michael P. Meredith, Andrew Clarke, Timothy D. Jickells, Paul Mann, and Helen Rossetti. 2010. 'Seasonal and interannual variation of dissolved iodine speciation at a coastal Antarctic site', Marine Chemistry, 118: 171-81.

Cuevas, C. A., N. Maffezzoli, J. P. Corella, A. Spolaor, P. Vallelonga, H. A. Kjaer, M. Simonsen, M. Winstrup, B. Vinther, C. Horvat, R. P. Fernandez, D. Kinnison, J. F. Lamarque, C. Barbante, and A. Saiz-Lopez. 2018. 'Rapid increase in atmospheric iodine levels in the North Atlantic since the mid-20th century', Nature Communications, 9: 6.

Cutter, G. A., J. G. Moffett, M. C. Nielsdottir, and V. Sanial. 2018. 'Multiple oxidation state trace elements in suboxic waters off Peru: In situ redox processes and advective/diffusive horizontal transport', Marine Chemistry, 201: 77-89.

Ducklow, H. W., M. R. Stukel, R. Eveleth, S. C. Doney, T. Jickells, O. Schofield, A. R. Baker, J. Brindle, R. Chance, and N. Cassar. 2018. 'Spring-summer net community production, new production, particle export and related water column biogeochemical processes in the marginal sea ice zone of the Western Antarctic Peninsula 2012-2014', Philosophical Transactions of the Royal Society a-Mathematical Physical and Engineering Sciences, 376: 15.

Edwards, A., and V. W. Truesdale. 1997. 'Regeneration of inorganic iodine species in Loch Etive, a natural leaky incubator', Estuarine Coastal and Shelf Science, 45: 357-66.

Elderfield, H., and V. W. Truesdale. 1980. 'On the biophilic nature of iodine in seawater', Earth and Planetary Science Letters, 50: 105-14.

Farrenkopf, A. M., and G. W. Luther. 2002. 'Iodine chemistry reflects productivity and denitrification in the Arabian Sea: evidence for flux of dissolved species from sediments of western India into the OMZ', Deep-Sea Research Part II-Topical Studies in Oceanography, 49: 2303-18.

Farrenkopf, A. M., G. W. Luther, V. W. Truesdale, and C. H. Van Der Weijden. 1997. 'Sub-surface iodide maxima: evidence for biologically catalyzed redox cycling in Arabian Sea OMZ during the SW intermonsoon', Deep Sea Research Part II: Topical Studies in Oceanography, 44: 1391-409.

Ganzeveld, L., D. Helmig, C. W. Fairall, J. Hare, and A. Pozzer. 2009. 'Atmosphere-ocean ozone exchange: A global modeling study of biogeochemical, atmospheric, and waterside turbulence dependencies', Global Biogeochemical Cycles, 23.

Ghose, N. C., K. Das, and D. Saha. 2003. 'Distribution of iodine in soil-water system in the Gandak basin, Bihar', Journal of the Geological Society of India, 62: 91-98.

Gilfedder, B. S., M. Petri, and H. Biester. 2007. 'Iodine speciation in rain and snow: Implications for the atmospheric iodine sink', Journal of Geophysical Research-Atmospheres, 112: 7.

Grand, Maxime M., Christopher I. Measures, Mariko Hatta, William T. Hiscock, William M. Landing, Peter L. Morton, Clifton S. Buck, Pamela M. Barrett, and Joseph A. Resing. 2015. 'Dissolved Fe and Al in the upper 1000 m of the eastern Indian Ocean: A high-resolution transect along 95°E from the Antarctic margin to the Bay of Bengal', Global Biogeochemical Cycles, 29: 375-96.

Hardacre, C., O. Wild, and L. Emberson. 2015. 'An evaluation of ozone dry deposition in global scale chemistry climate models', Atmospheric Chemistry and Physics (Print), 15: 6419-36.

Hardisty, D. S., T. J. Horner, S. D. Wankel, J. Blusztajn, and S. G. Nielsen. 2020. 'Experimental observations of marine iodide oxidation using a novel sparge-interface MC-ICP-MS technique', Chemical Geology, 532: 119360.

Hou, Xiaolin, Ala Aldahan, Sven P. Nielsen, Goran Possnert, Hartmut Nies, and Jim Hedfors. 2007. 'Speciation of I-129 and I-127 in seawater and implications for sources and transport pathways in the North Sea', Environmental Science & Technology, 41: 5993-99.

910 Hughes, C., E. Barton, H. Hepach, R. Chance, M. Pickering, and K. Hogg. 2020. 'Iodate
911 production in marine ammonium-oxidising bacteria', *Manuscript to be submitted to*
912 *Global Biogeochemical Cycles*.
913 Jickells, T. D., S. S. Boyd, and A. H. Knap. 1988. 'Iodine cycling in the Sargasso Sea and the
914 Bermuda Inshore waters', Marine Chemistry, 24: 61-82.
915 Johannessen, T., and E. Dahl. 1996. 'Declines in oxygen concentrations along the Norwegian
916 Skagerrak coast, 1927-1993: A signal of ecosystem changes due to eutrophication?',
917 Limnology and Oceanography, 41: 766-78.
918 Longhurst, A.R. 1998. Ecological geography of the sea (Academic: San Diego).
919 Lu, Wanyi, Andy Ridgwell, Ellen Thomas, Dalton S. Hardisty, Genming Luo, Thomas J.
920 Algeo, Matthew R. Saltzman, Benjamin C. Gill, Yanan Shen, Hong-Fei Ling, Cole T.
921 Edwards, Michael T. Whalen, Xiaoli Zhou, Kristina M. Gutchess, Li Jin, Rosalind E.
922 M. Rickaby, Hugh C. Jenkyns, Timothy W. Lyons, Timothy M. Lenton, Lee R. Kump,
923 and Zunli Lu. 2018. 'Late inception of a resiliently oxygenated upper ocean', Science:
924 eaar5372.
925 Luther, G. W., C. B. Swartz, and W. J. Ullman. 1988. 'Direct determination of iodide in
926 seawater by cathodic stripping square-wave voltammetry', Analytical Chemistry, 60:
927 1721-24.
928 MacDonald, S. M., J. C. Gómez Martín, R. Chance, S. Warriner, A. Saiz-Lopez, L. J.
929 Carpenter, and J. M. C Plane. 2014. 'A laboratory characterisation of inorganic iodine
930 emissions from the sea surface: dependence on oceanic variables and parameterisation
931 for global modelling', Atmospheric Chemistry and Physics, 14: 5841-52.
932 Mahajan, Anoop S., Liselotte Tinel, Shrivardhan Hulswar, Carlos A. Cuevas, Shanshan Wang,
933 Sachin Ghude, Ravidas K. Naik, Rajani K. Mishra, P. Sabu, Amit Sarkar, N.
934 Anilkumar, and Alfonso Saiz Lopez. 2019. 'Observations of iodine oxide in the Indian
935 Ocean marine boundary layer: A transect from the tropics to the high latitudes',
936 Atmospheric Environment: X, 1: 100016.
937 McFiggans, G., H. Coe, R. Burgess, J. Allan, M. Cubison, M. R. Alfarra, R. Saunders, A. Saiz-
938 Lopez, J. M. C. Plane, D. J. Wevill, L. J. Carpenter, A. R. Rickard, and P. S. Monks.
939 2004. 'Direct evidence for coastal iodine particles from Laminaria macroalgae - linkage
940 to emissions of molecular iodine', Atmospheric Chemistry and Physics, 4: 701-13.
941 Moran, Jean E., Sarah D. Oktay, and Peter H. Santschi. 2002. 'Sources of iodine and iodine
942 129 in rivers', Water Resources Research, 38: 24-1-24-10.
943 Moriyasu, Rintaro, Zachary C. Evans, Kenneth M. Bolster, Dalton S. Hardisty, and James W.
944 Moffett. 2020. 'The Distribution and Redox Speciation of Iodine in the Eastern Tropical
945 North Pacific Ocean', Global Biogeochemical Cycles, 34: e2019GB006302.
946 Nakayama, E., T. Kimoto, K. Isshiki, Y. Sohrin, and S. Okazaki. 1989. 'Determination and
947 distribution of iodide-iodine and total-iodine in the north Pacific ocean by using a new
948 automated electrochemical method', Marine Chemistry, 27: 105-16.
949 Naqvi, S. W. A., D. A. Jayakumar, P. V. Narvekar, H. Naik, V. V. S. S. Sarma, W. D'Souza,
950 S. Joseph, and M. D. George. 2000. 'Increased marine production of N2O due to
951 intensifying anoxia on the Indian continental shelf', Nature, 408: 346.
952 Orsi, Alejandro H., Thomas Whitworth, and Worth D. Nowlin. 1995. 'On the meridional extent
953 and fronts of the Antarctic Circumpolar Current', Deep Sea Research Part I:
954 Oceanographic Research Papers, 42: 641-73.
955 Prados-Roman, C., C. A. Cuevas, T. Hay, R. P. Fernandez, A. S. Mahajan, S. J. Royer, M.
956 Galí, R. Simó, J. Dachs, K. Großmann, D. E. Kinnison, J. F. Lamarque, and A. Saiz-
957 Lopez. 2015. 'Iodine oxide in the global marine boundary layer', Atmospheric
958 Chemistry and Physics (Print), 15: 583-93.

Sadasivan, S., and S. J. S. Anand. 1979. 'Chlorine, bromine and iodine in monsoon rains in India', Tellus, 31: 290-94.
Sarwar, G., D. W. Kang, K. Foley, D. Schwede, B. Gantt, and R. Mathur. 2016. 'Technical note: Examining ozone deposition over seawater', Atmospheric Environment, 141: 255-62.
Schlitzer, R. 2014. "Ocean Data View." In.: http://odv.awi.de.
Schwehr, K. A., and P. H. Santschi. 2003. 'Sensitive determination of iodine species, including organo-iodine, for freshwater and seawater samples using high performance liquid chromatography and spectrophotometric detection', Analytica Chimica Acta, 482: 59-71.
Sherwen, T., M. J. Evans, R. Sommariva, L. D. J. Hollis, S. M. Ball, P. S. Monks, C. Reed, L. J. Carpenter, J. D. Lee, G. Forster, B. Bandy, C. E. Reeves, and W. J. Bloss. 2017. 'Effects of halogens on European air-quality', Faraday Discussions, 200: 75-100.
Sherwen, T.S., L. Tinel, R. Chance, L.J. Carpenter, and M.J. Evans. 2019. 'Re-approaching global iodine emissions: A novel parameterisation for sea-surface iodide concentrations using a machine learning approach. In prep.'.
Truesdale, V. W. 1978. 'Iodine in inshore and off-shore marine waters', Marine Chemistry, 6: 1-13.
Truesdale, V. W., A. J. Bale, and E. M. S. Woodward. 2000. 'The meridional distribution of dissolved iodine in near-surface waters of the Atlantic Ocean', Progress in Oceanography, 45: 387-400.
Truesdale, V. W., D. S. Danielssen, and T. J. Waite. 2003. 'Summer and winter distributions of dissolved iodine in the Skagerrak', Estuarine Coastal and Shelf Science, 57: 701-13.
Truesdale, V. W., and C. P. Spencer. 1974. 'Studies on the determination of inorganic iodine in seawater', Marine Chemistry, 2: 33-47.
Tsunogai, S. 1971. 'Iodine in the deep water of the ocean', Deep-Sea Research, 18: 913-19.
Tsunogai, S., and T. Henmi. 1971. 'Iodine in the surface water of the Pacific Ocean', Journal of the Oceanographical Society of Japan, 27: 67-72.
Vinayachandran, P. N., Adrian J. Matthews, K. Vijay Kumar, Alejandra Sanchez-Franks, V. Thushara, Jenson George, V. Vijith, Benjamin G. M. Webber, Bastien Y. Queste, Rajdeep Roy, Amit Sarkar, Dariusz B. Baranowski, G. S. Bhat, Nicholas P. Klingaman, Simon C. Peatman, C. Parida, Karen J. Heywood, Robert Hall, Brian King, Elizabeth C. Kent, Anoop A. Nayak, C. P. Neema, P. Amol, A. Lotliker, A. Kankonkar, D. G. Gracias, S. Vernekar, A. C. D'Souza, G. Valluvan, Shrikant M. Pargaonkar, K. Dinesh, Jack Giddings, and Manoj Joshi. 2018. 'BoBBLE: Ocean–Atmosphere Interaction and Its Impact on the South Asian Monsoon', Bulletin of the American Meteorological Society, 99: 1569-87.
Wadley, M.R., D.P. Stevens, T.D. Jickells, C. Hughes, A.R. Baker, R.J. Chance, H. Hepach, L. Tinel, and L.J. Carpenter. 2020. 'A Global Model for Iodine Speciation in the Upper Ocean', Global Biogeochemical Cycles, Resubmitted manuscript.
Waite, T. J., V. W. Truesdale, and J. Olafsson. 2006. 'The distribution of dissolved inorganic iodine in the seas around Iceland', Marine Chemistry, 101: 54-67.
Wang, F., A. Saiz-Lopez, A. S. Mahajan, J. C. Gómez Martín, D. Armstrong, M. Lemes, T. Hay, and C. Prados-Roman. 2014. 'Enhanced production of oxidised mercury over the tropical Pacific Ocean: a key missing oxidation pathway', Atmospheric Chemistry and Physics (Print), 14: 1323-35.
Wong, G. T. F. 2001. 'Coupling iodine speciation to primary, regenerated or "new" production: a re-evaluation', Deep-Sea Research Part I-Oceanographic Research Papers, 48: 1459-76.

1008 Wong, G. T. F., and X. H. Cheng. 1998. 'Dissolved organic iodine in marine waters:
1009 Determination, occurrence and analytical implications', Marine Chemistry, 59: 271-81.
1010 Wong, G. T. F., and L. S. Zhang. 2003. 'Geochemical dynamics of iodine in marginal seas: the
1011 southern East China Sea', Deep-Sea Research Part II-Topical Studies in Oceanography,
1012 50: 1147-62.
1013 Zic, V., M. Caric, and I. Ciglenecki. 2013. 'The impact of natural water column mixing on
1014 iodine and nutrient speciation in a eutrophic anchialine pond (Rogoznica Lake,
1015 Croatia)', Estuarine Coastal and Shelf Science, 133: 260-72.
1016

Figures

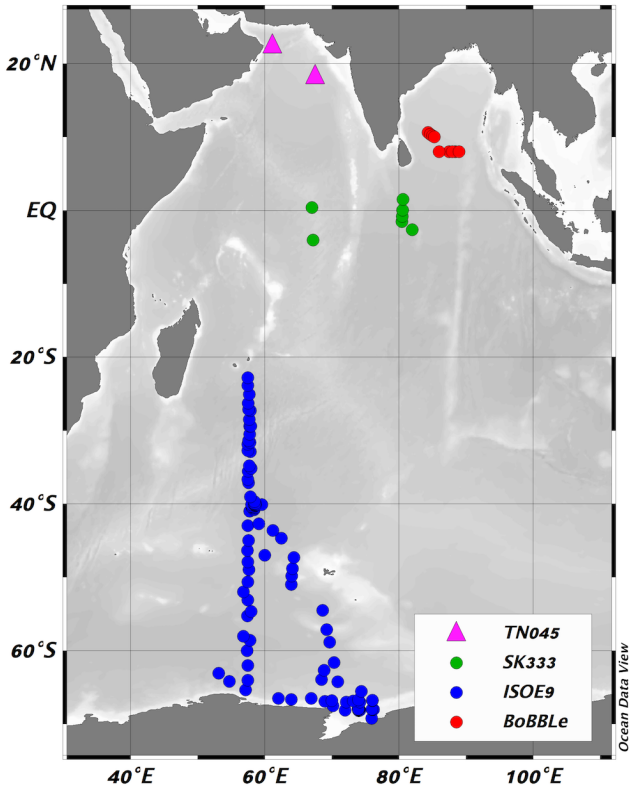

Figure 1. Locations of new sea surface iodide observations made during this work, coloured according to cruise (green – SK333, red – BoBBLe, blue – ISOE9) and previous observations from the region made by Farrenkopf et al., 2002, and included in the compilation of Chance et al., 2014 (pink triangles). Figure produced using Ocean Data View (Schlitzer 2014).

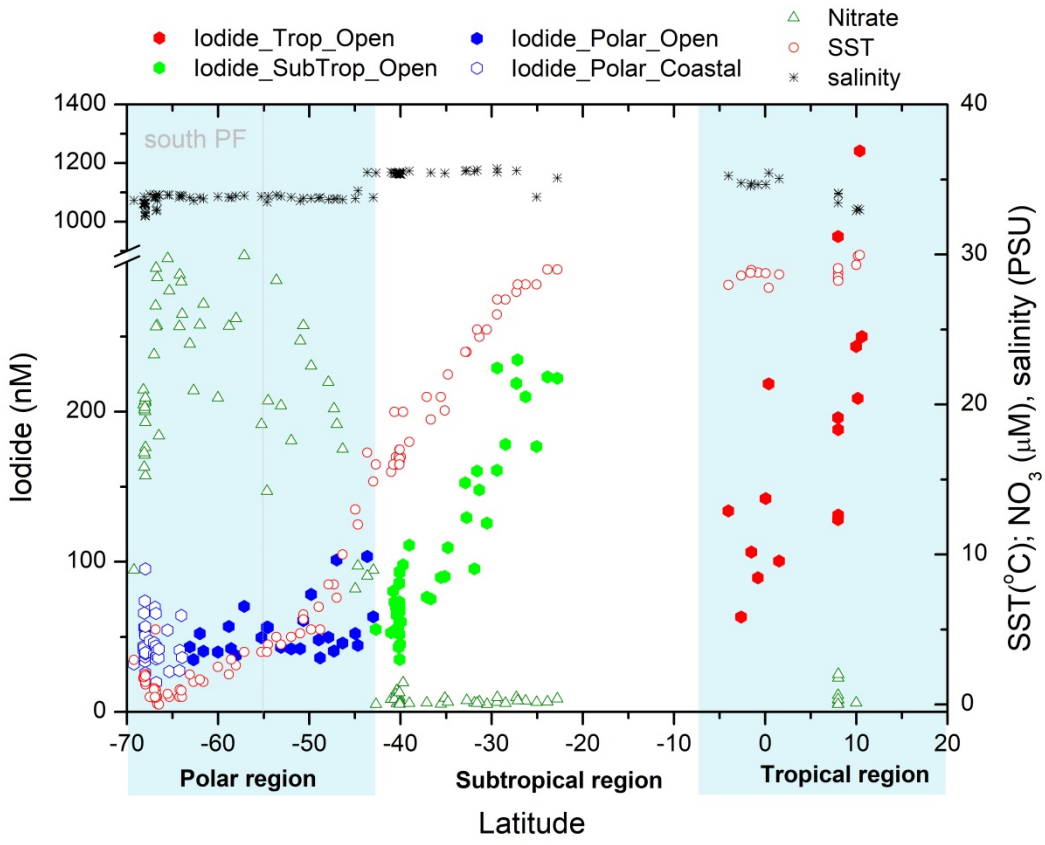

Figure 2. Latitudinal variation of surface iodide concentrations in nM observed in the open Indian and Southern Ocean (●) and in the coastal Southern Ocean (o) compared to the observed sea surface temperature (˚C), salinity (PSU) and nitrate concentrations (μM). Boxes indicate the three different oceanographic regimes considered in the text. The dotted grey line indicates the position of the Polar Front (PF).

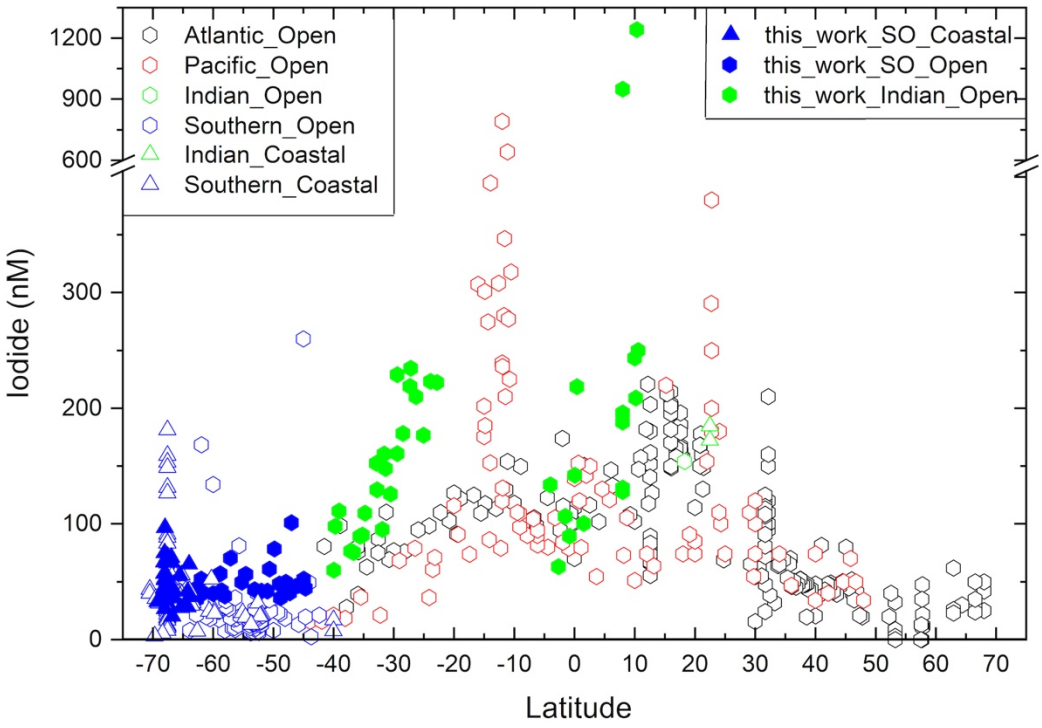

Figure 3. Latitudinal variation of sea surface iodide concentrations in the Indian (green) and Indian sector of the Southern Ocean (SO; blue), compared to other ocean basins (Atlantic – black, Pacific – red). New observations made as part of this work are shown with filled symbols, while other values (see compilation of (Chance, Tinel, Sherwen, Baker, Bell, Brindle, Campos, Croot, Ducklow, He, Hopkins, et al. 2019)) are shown in hollow symbols. Division between ocean basins follows the borders proposed by the World Ocean Circulation Experiment (https://www.nodc.noaa.gov/woce/woce_v3/wocedata_1/woce-uot/summary/bound.htm), and (Orsi, Whitworth, and Nowlin 1995) for the Southern Ocean.

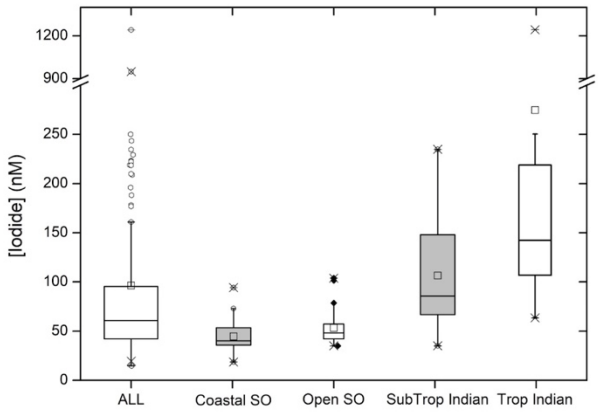

Figure 4. Box and Whisker plot showing descriptive statistics for the entire data set ('ALL'; n=127) and sub-divided into the following regions: polar coastal waters ('Coastal SO'; n=38), open waters of the Southern Ocean ('Open SO'; n=27), the Indian Ocean subtropical convergence zone and southern subtropical gyre ('SubTrop Indian'; n=46 and the tropical Indian Ocean ('Trop Indian'; n=16). See main text for more detailed descriptions of these categories. Centre lines show the medians; squares are the means; box limits indicate the 25th and 75th percentiles; whiskers extend 1.5 times the interquartile range from the 25th and 75th percentiles, outliers are represented by dots; crosses represent 1st and 99th percentiles; width of the boxes is proportional to the square root of the sample size.

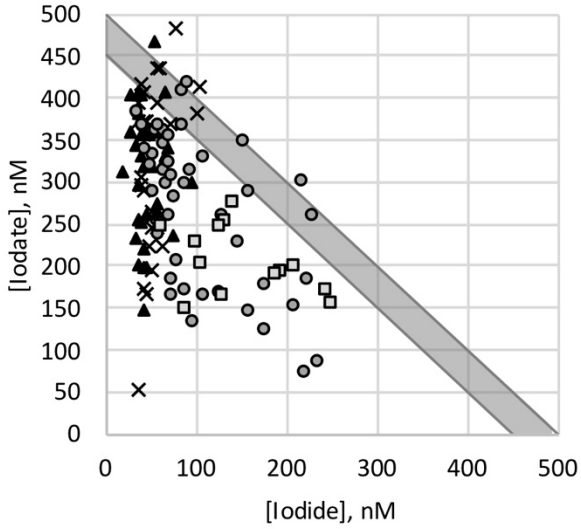

Figure 5. Sea surface iodate concentrations plotted against iodide concentrations, for samples from polar coastal waters (▲), open waters of the Southern Ocean (×), the Indian Ocean subtropical convergence zone and southern subtropical gyre (○) and the tropical Indian Ocean (□). Grey line shows 1:1 relationship, assuming a total inorganic iodine concentration of 450 to 500 nM (Chance et al. 2014). Note for clarity two samples with very high iodide concentrations not shown.

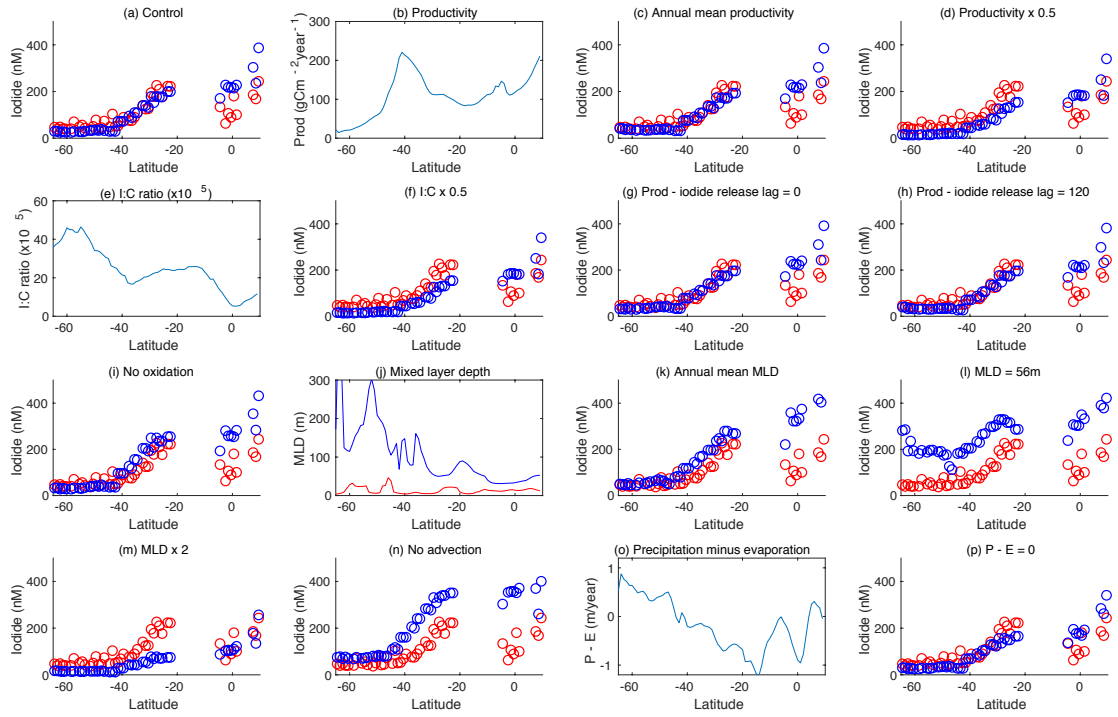

Figure 6. Results from model process sensitivity experiments. (a) Observed (red) and model (blue) iodide concentrations as a function of latitude, in the Indian Ocean and the Indian sector of the Southern Ocean along a section at 60°E (note observed iodide over 500nM have been excluded here) (b) observed primary productivity (Behrenfeld and Falkowski 1997) as a function of latitude, (c) iodide with the seasonal cycle of productivity replaced with the annual mean, (d) iodide with seasonal productivity halved, (e) the model I:C ratio, (f) iodide with the model I:C ratio halved, (g) iodide with iodide release from plankton at the same time as carbon assimilation, (h) iodide with iodide release from plankton lagged 120 days from carbon assimilation, (i) no mixed layer oxidation of iodide, (j) maximum (blue) and minimum (red) mixed layer depth from the OCCAM model (Aksenov et al., 2010) as a function of latitude, (k) iodide with the seasonal cycle of mixed layer depth replaced with the annual mean, (l) iodide with the seasonal cycle of mixed layer depth replaced by the constant global mean of 56m, (m) seasonal MLD doubled, (n) no vertical or horizontal advection, (o) P-E from the OCCAM model (Aksenov et al. 2010) as a function of latitude, (p) P-E set to zero.

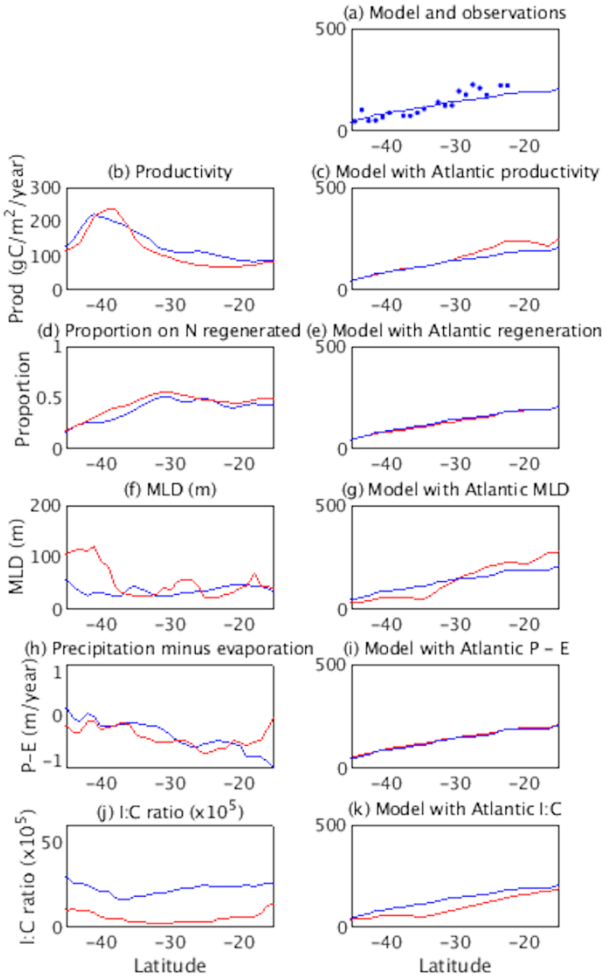

Figure 7. Impact of imposing Atlantic forcings in the Indian Ocean basin in the iodine cycling model. Plots are annual mean iodide for 57°E in the Indian Ocean. (a) observed (dots) and modelled (line) iodide, in nM (b,d,f,h, j) latitudinal sections for each process-related quantity for the Indian (blue) and Atlantic (red) Oceans, (c,e,g,i, k) corresponding latitudinal sections of iodide for control (blue) and Atlantic forcing imposed over the Indian basin (red).

Tables

Table 1. Regression parameters for relationships between iodide (in nM) and latitude, SST and nitrate concentration. For each variable, top row gives results of Pearsons Product-Moment correlation (parametric) and bottom row gives results of Spearmans rank correlation (non-parametric). Statistically significant ($p < 5\%$) correlations are shown in bold. *Two extremely high iodide concentrations in tropical sub-set excluded from correlation analysis.

Independent variable	R^2 ρ_s	*slope* -	*intercept* -	*p* *p*
|latitude|				
All data	0.24	-3.4	251	**5×10^{-9}**
	-0.74	-	-	**0**
Sub-tropical	0.86	-9.5	449	**3×10^{-20}**
	-0.83	-	-	**1.1×10^{-12}**
Southern Ocean	0.10	-0.64	87	**0.01**
	-0.21	-	-	**9.6×10^{-3}**
*Tropical**	0.39	9.2	109	**0.02**
	0.59	-	-	**1.7×10^{-2}**
Chance et al., 2014	0.40	-2.7	200	**<0.05**
	-0.65	-	-	**<0.05**
SST (°C)				
All data	0.26	5.7	21	**1×10^{-9}**
	0.81	-	-	**0**
Sub-tropical	0.89	11.8	-130	**2×10^{-22}**
	0.87	-	-	**6.7×10^{-15}**
Southern Ocean	0.15	1.8	43	**0.002**
	0.35	-	-	**4.2×10^{-3}**
*Tropical**	0.14	37	901	0.2
	0.42	-	-	0.14
Chance et al., 2014	0.52	5.7	4	**<0.05**
	0.72	-	-	**<0.05**
[Nitrate], µM				
All data	0.17	-3.9	136	**3×10^{-5}**
	-0.58	-	-	**1.6×10^{-10}**
Sub-tropical	0.004	-13	118	0.7
	-0.02	-	-	0.93
Southern Ocean	0.03	-0.53	61	0.2
	-0.13	-	-	0.34
Tropical (n=5)	0.21	-31	195	0.4
	-0.14	-	-	0.79
Chance et al., 2014	0.36	-5.2	125	**<0.05**
	-0.73	-	-	**<0.05**

Supplementary Information

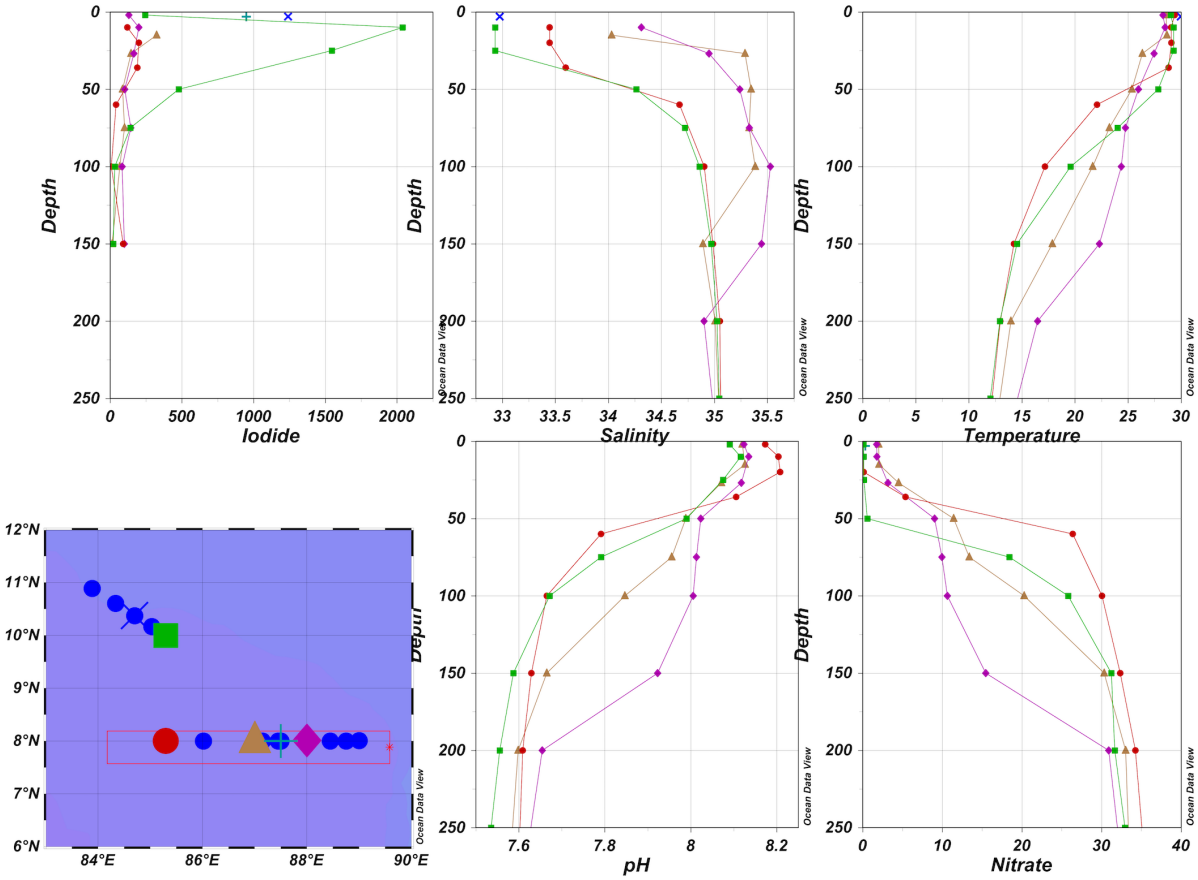

Figure S1. Selected depth profile data from the BoBBLe cruise in the Bay of Bengal, showing exceptionally high surface and subsurface iodide concentrations. Station AR shown in green squares, underway samples BS3 and BS8 shown by blue cross and green plus sign. Note the high salinity core of Summer Monsoon Current (SMC) evident in stations with purple & brown symbols. Figure prepared using Ocean Data View (Schlitzer 2014).

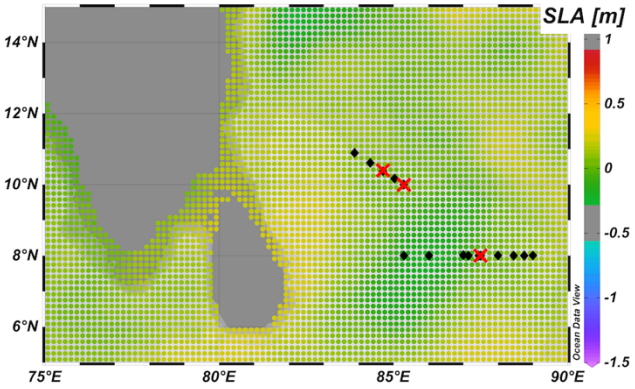

Figure S2. Sea surface height anomaly (SLA, m) for 26-30 June 2016 and BoBBLe station positions, with high iodide stations indicated by red crosses. Green areas show negative sea level anomalies, where upwelling is taking place, indicative of Sri Lanka Dome area. Dataset (Zlotnicki, Qu, and Willis 2016) accessed [2017-01-21] at https://doi.org/10.5067/SLREF-CDRV1. Figure prepared using Ocean Data View (Schlitzer 2014).

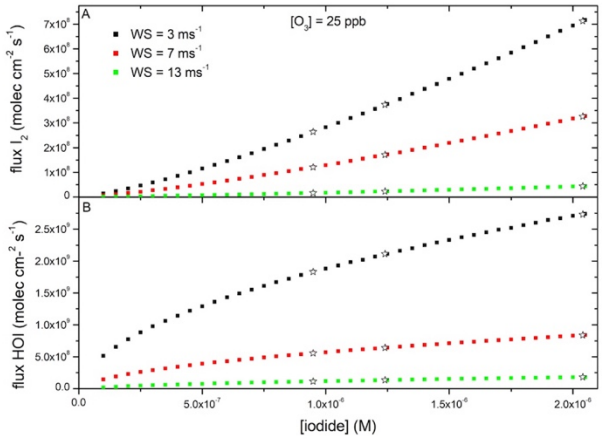

Figure S3: Predicted fluxes for HOI and I_2 emissions (molecules cm^{-2} s^{-1}) as a function of the aqueous iodide concentration (M) for a fixed ozone concentration of 25 ppb and three different wind speeds (black: 3 ms^{-1}, red: 7 ms^{-1}, green: 13 ms^{-1}), calculated using the parametrisation in (Carpenter et al. 2013). The stars symbols show the predicted fluxes for the high (>600nM) iodide concentrations measured in the tropical Indian Ocean during the BoBBLe cruise.

Table S1. Gradients of sea surface iodide concentrations against latitude and sea surface temperature (SST) for open ocean subtropical waters (defined by province) of the global ocean basins. Iodide data from (Chance, Tinel, Sherwen, Baker, Bell, Brindle, Campos, Croot, Ducklow, He, Hopkins, et al. 2019) and sea surface temperatures from the World Ocean Atlas 2013 (Locarnini et al. 2013).

		$[I^-]$ vs |Latitude|		**$[I^-]$ vs. SST**		**Modal month**	**% Frequency of modal month**
	n	slope	R^2	slope	R^2		
North Atlantic	123	-3.5	0.40	12.2	0.47	11	39
South Atlantic	27	-2.2	0.60	6.3	0.60	10	70
North Pacific	24	-3.5	0.06	9.9	0.24	3	38
South Pacific	27	-14.3	0.40	6.6	0.01	11	37
South pacific ex. Cutter et al	10	-2.8	0.59	6.7	0.65	1	90
South Indian	46	-9.5	0.85	13.3	0.84	1	67
South Indian, modelled	--	-5.5	0.99	--	--	--	--

References

Carpenter, L. J., S. M. MacDonald, M. D. Shaw, R. Kumar, R. W. Saunders, R. Parthipan, J. Wilson, and J. M. C. Plane. 2013. 'Atmospheric iodine levels influenced by sea surface emissions of inorganic iodine', Nature Geoscience, 6: 108-11.

Chance, R.J., L. Tinel, T. Sherwen, A. Baker, T. Bell, J. Brindle, M.L.A.M. Campos, P. Croot, H. Ducklow, P. He, B. Hoogakker, F.E. Hopkins, C. Hughes, T. Jickells, D. Loades, D.A. Reyes Macaya, A.S. Mahajan, G. Malin, D.P. Phillips, A.K. Sinha, A. Sarkar, I.J. Roberts, R. Roy, X. Song, H.A. Winklebauer, K. Wuttig, M. Yang, P. Zhou, and L.J. Carpenter. 2019. "Global sea-surface iodide observations, 1967-2018." In. British Oceanographic Data Centre - Natural Environment Research Council, UK.

Locarnini, R. A., A.V. Mishonov, J.I. Antonov, T.P. Boyer, H.E. Garcia, O.K. Baranova, M.M. Zweng, C.R. Paver, J.R. Reagan, D.R. Johnson, M. Hamilton, and D. Seidov. 2013. "World Ocean Atlas 2013, Volume 1: Temperature." In, edited by S. Levitus and A. Mishonov, 40. Washington, D.C.: U.S. Government Printing Office.

Schlitzer, R. 2014. "Ocean Data View." In.: http://odv.awi.de.

Zlotnicki, V., Z. Qu, and J. Willis. 2016. "JPL MEaSUREs Gridded Sea Surface Height Anomalies Version 1609." In, edited by NASA Physical Oceanography DAAC. NASA Physical Oceanography DAAC.